Regime shifts in bistable water-stressed ecosystems due to amplification of stochastic rainfall patterns

Luis Cueto-Felgueroso,[1,2,*] Marco Dentz,[3] and Ruben Juanes[2]

[1]*Department of Hydraulics, Energy and the Environment, Technical University of Madrid (UPM), Spain*

[2]*Department of Civil and Environmental Engineering, Massachusetts Institute of Technology, Cambridge, Massachusetts, USA*

[3]*Spanish National Research Council (IDAEA-CSIC), Barcelona, Spain*

(Received 21 October 2014; revised manuscript received 13 April 2015; published 28 May 2015)

We develop a framework that casts the point water-vegetation dynamics under stochastic rainfall forcing as a continuous-time random walk (CTRW), which yields an evolution equation for the joint probability density function (PDF) of soil-moisture and biomass. We find regime shifts in the steady-state PDF as a consequence of changes in the rainfall structure, which flips the relative strengths of the system attractors, even for the same mean precipitation. Through an effective potential, we quantify the impact of rainfall variability on ecosystem resilience and conclude that amplified rainfall regimes reduce the resilience of water-stressed ecosystems, even if the mean annual precipitation remains constant.

DOI: 10.1103/PhysRevE.91.052148 PACS number(s): 05.40.−a, 87.10.Mn, 05.45.−a

I. INTRODUCTION

The amplification of the hydrologic cycle, characterized by more extreme precipitation regimes, is one of the major concerns associated with global warming [1,2]. Models and datasets suggest that global warming is affecting land-atmosphere feedbacks, altering the hydrologic cycle [3], and leading to more extreme rainfall regimes [4–7], with intense individual events and longer dry periods between them. Understanding the response of terrestrial ecosystems to these changes is a challenging, open problem [8]. The frequency and intensity of precipitation events, not just aggregate measures such as mean precipitation rate, are important determinants of the structure and function of terrestrial ecosystems, as revealed by the analysis of fractional woody cover in Africa [9] and by the patterns of tropical tree cover [10]. These observations of the impact of rainfall patterns on the relative distribution and dominance of competing plant life forms are consistent with simulations predicting a higher risk of drought and runoff under intensified rainfall regimes [2] and point to complex interactions between stochastic climate and environmental and biological factors.

Characterizing resilience is essential in the assessment of ecological services in a changing environment [11,12]. Natural systems exhibit properties of strongly coupled systems; abrupt changes in the climate system [13] and global terrestrial biomes [11,14–18] are often interpreted as shifts between alternative stable equilibria of nonlinear dynamical systems. The idea of multiple equilibrium states has a long tradition in the analysis of vegetation dynamics, rationalizing coexistence, competition and optimality in the observed patterns of vegetation cover [19,20]. The striking merit of this idea is that complex interactions are captured by a minimal-ingredients conceptual model describing the feedbacks between climate and biogeochemical factors. Understanding the structure of transitions between stable states, and identifying potential early-warning signals, has recently emerged as a central scientific problem in a scenario of increased anthropogenic forcing [17,18,21].

Water-stressed environments are susceptible to structural shifts in response to changes in rainfall and temperature, and to environmental disturbances, natural and/or anthropogenic [16,17,22–24]; multistability explains the patterns of tree cover distribution along precipitation gradients, suggesting that treeless areas, savannas, and tropical forests may represent alternative stable states separated by critical transitions [19,25,26]. In the presence of multiple equilibria, disturbances or slow changes in environmental forcing may trigger catastrophic shifts to a degraded state of the ecosystem. The role of random perturbations on bistable dynamical systems has been studied theoretically in the context of population dynamics [27,28], climate modeling [29,30], and soil moisture-vegetation dynamics with simple rainfall forcing [31,32]. Rainfall variability has been shown to alter the statistical properties of the coupled water-vegetation system. In particular, interannual fluctuations of precipitation may led to the emergence of an intermediate statistically stable condition between the two stable states of the deterministic dynamics of vegetation [31]. This type of noise-induced stabilization has also been identified in models of population dynamics [33]. Seasonality in rainfall leads to regime switching between the two alternative states of the system [32], while rainfall intermittency may increase the resilience of the system [34]. Soil-atmosphere feebacks (soil moisture-rainfall feedbacks) may also lead to multimodality of the soil moisture probability density functions [35–38].

There are strong indications that global climate change is amplifying rainfall patterns and leading to stronger and less frequent precipitation events, even if the mean annual precipitation remains unchanged. This naturally poses the question of whether this amplified rainfall regime may affect, perhaps catastrophically, ecosystems that already exhibit alternative stable states.

Here we present a probabilistic framework that clearly identifies and systematically quantifies the role of stochastic rainfall patterns on the resilience of bistable water-stressed ecosystems. The stochastic system dynamics are described by the evolution equation for the joint probability density function (PDF) of soil moisture and vegetation biomass, which quantifies the likelihood of observing the system at a particular state, given the environmental conditions and

*luis.cueto@upm.es

rainfall forcing. Soil moisture is the key variable to understand the spatiotemporal link between hydrologic and ecological patterns and processes [22,39,40]. The proposed model takes as a starting point a probabilistic framework [41–44], which has led to fundamental advances in the understanding of the dynamics of soil moisture [42,43] and the water-vegetation coupling [45,46] under stochastic rainfall.

The proposed stochastic approach is based on a deterministic dynamic system, which describes the coupling between soil water and vegetation dynamics. Stochastic rainfall forcing is modeled as a renewal process characterized by an arbitray interstorm waiting time distribution. This stochastic model can be cast in the form of a continuous-time random walk (CTRW) [47,48] that is characterized by a nonlinear propagation of the saturation and biomass states between the turning points, which are defined by the storm events. The CTRW approach provides a general and powerful framework for the modeling of dynamic systems in the presence of broad distributions of characteristic time scales [49,50]. Thus, the stochastic model presented here is valid for a wide range of point-process descriptions of rainfall such as fractional Poisson processes [51].

While the impact of rainfall statistics on the PDF of soil moisture has been extensively characterized in the literature [43], the structure of the joint PDF of soil water and vegetation has not. The presented analysis demonstrates that the rainfall statistics, not just the mean annual precipitation, control the structural properties of the joint PDF, including the connection between bistability of the underlying deterministic dynamics and bimodality of the joint PDF. This observation is the key to understanding the impact of an intensified hydrologic cycle on the resilience and stability of water-stressed ecosystems. We define an effective potential function [29,35,36] to quantify the impact of rainfall variability on ecosystem stability. This analysis shows that resilience decreases with increasing intensification of the hydrologic cycle. Our results point to the need to view global datasets of climate, soil moisture, and vegetation in terms of both aggregate precipitation measures and the patterns of inter- and intraannual rainfall variability.

II. DETERMINISTIC DYNAMIC SYSTEM

The deterministic dynamics of the coupled evolution of soil-water saturation, $S[\mathrm{m}^0]$, and plant biomass density, $B[\mathrm{kg\,m}^{-2}]$, at the daily time scale, are described by the coupled nonlinear equations

$$\frac{dS}{dt} = -\sigma(S,B) + I, \tag{1a}$$

$$\frac{dB}{dt} = \beta(S,B). \tag{1b}$$

In this minimal model of water-vegetation coupling, the dynamics of soil moisture and biomass are driven by deterministic drift terms. We make here the following choice for σ and β:

$$\sigma = \frac{1}{\phi Z_r}\left(\frac{ES}{S+k} + \frac{\beta SB}{S+k} + K_s S^2\right), \tag{2a}$$

$$\beta = \frac{\gamma SB}{S+k} - \frac{\mu B}{B+b_0} - \delta B^2. \tag{2b}$$

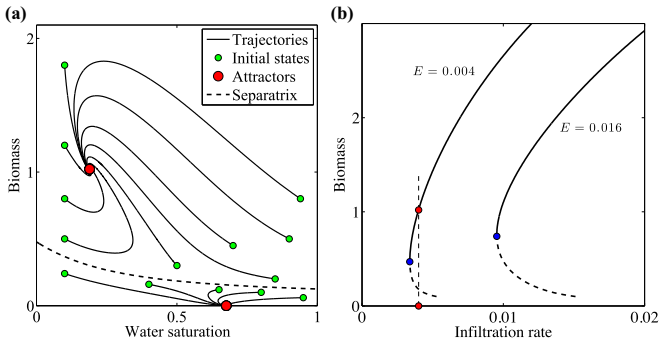

FIG. 1. (Color online) Behavior of the deterministic system [Eqs. (1a) and (1b)]. The dynamical system is deterministic when the infiltration rate is constant, and the Gaussian noise terms are neglected. For parameter values that are typical of arid and semiarid environments, the system exhibits two alternative stable states. (a) Sample trajectories for $E = 0.004$, $I = 0.004$. Furthermore, we set $\beta = 0.004$, $\gamma = 0.02$, $\delta = 0.004$, $\mu = 0.008$, $k = 0.2$, $b_0 = 0.4$, and $K_s = 0.002$. The system is bistable, and we may arrive at either of the attractors depending on the initial condition. The region of initial values in phase space that converges to a given attractor is called the basin of attraction of that stable point. (b) Bifurcation diagrams using the recharge rate, I, as the bifurcation parameter. The two curves represent the biomass at equilibrium that corresponds to two evaporation rates, $E = 0.004$ and $E = 0.016$. For small infiltration rates, the system has two alternative stable states: a vegetated and a nonvegetated state (red dots).

Thus, the water balance Eq. (1a) includes losses from evaporation, first term in Eq. (2a), plant transpiration (second term), and drainage to deeper soil layers (third term), as well as a constant recharge from infiltration I [39,43,52]. Runoff is implicitly included through the constraint $S \leqslant 1$. Runoff losses for $S \leqslant 1$ are not considered explicitly. The biomass dynamics Eq. (2b) account for plant growth through the first term in Eq. (2b) and death (third term), as well as herbivore grazing (second term) [15,23,24,28,45,46]. Note that this choice of the grazing terms leads to bistability of the joint saturation-biomass system as discussed in the following and illustrated in Fig. 1.

The deterministic model Eq. (1) defines aggregate variables at the daily scale, in accordance with upscaled data obtained with detailed simulations at the hourly level [46]. The model parameters for the soil-water dynamics Eq. (2a) are the effective root depth, $Z_r[\mathrm{m}]$, the soil porosity, $\phi[\mathrm{m}^0]$, the maximum evaporation rate, $E[\mathrm{m\,day}^{-1}]$, the potential transpiration rate, $\beta[\mathrm{m}^3\mathrm{day}^{-1}\mathrm{kg}^{-1}]$, and the saturated hydraulic conductivity of the soil, $K_s[\mathrm{m\,day}^{-1}]$. Effective rainfall, or infiltration is modeled by the constant rate $I[\mathrm{day}^{-1}]$ in Eq. (1a), which corresponds to the fraction of rainfall that is neither intercepted by the vegetation canopy, nor lost due to runoff. In the biomass dynamics Eq. (2b), $\gamma[\mathrm{day}^{-1}]$ is the specific growth rate, $\mu[\mathrm{kg\,m}^{-2}\mathrm{day}^{-1}]$ is the grazing rate, and $\delta[\mathrm{kg}^{-1}\mathrm{m}^2\mathrm{day}^{-1}]$ is the death rate.

For a given set of parameters, soil moisture S and biomass B evolve from their initial states toward equilibrium values or *attractors* that can be obtained from a linear stability analysis [14,53]. For parameters that are typical of arid and

semiarid conditions [46], the model Eq. (1) exhibits alternative stable states: a vegetated state (S_v, B_v) and a nonvegetated one (S_{nv}, B_{nv}), as illustrated in Fig. 1(a). The sets of initial states converging toward the respective attractor, the *basins of attraction*, are separated by a line, the *separatrix*.

Basins of attraction emerge as fundamental concepts to characterize resilience in the classical analysis of climate and vegetation systems as deterministic coupled processes. Multiple equilibria are observed frequently in vegetation dynamics due to feedbacks between plant biomass and herbivore population [14,15], or as an expression of competition [19] or optimality [20]. Their ecological significance is clear: environmental disturbances may drive the system toward the basin of attraction of the alternative equilibrium, triggering an abrupt shift to that state. Bistability in nonlinear systems is also linked to the existence of tipping points in the system dynamics [17,18,21].

Using the infiltration rate as a bifurcation parameter, the vegetation biomass at equilibrium decreases with infiltration rate, until the system collapses to a nonvegetated state as shown in Fig. 1(b). For a range of infiltration rates both stable equilibria coexist, and shifts between them are possible due to environmental disturbances. Bistability in coupled climate-ecological systems has been proposed as an explanation for catastrophic shifts in natural systems [15,17,18,25]. A large body of literature has been devoted to characterizing these critical transitions and identifying early-warning signals [17,18,21]. The impact of environmental perturbations, and stochasticity in the driving forces and subsequent shifts between the stable states, cannot be captured, however, by the deterministic model Eq. (1).

For completeness, we give here the evolution equation of the joint distribution $p(s,b,t)$ for the deterministic system Eq. (1). The PDF $p(s,b,t)$ is governed by the Liouville equation,

$$\frac{\partial p}{\partial t} - \frac{\partial}{\partial s}(\sigma - I)\, p + \frac{\partial}{\partial b}\beta p = 0. \tag{3}$$

For a given initial distribution $p_0(s,b) = p(s,b,t=0)$, the joint PDF $p(s,b,t)$ evolves toward the steady-state PDF,

$$p_\infty(s,b) = \chi_v \delta(s - S_v)\delta(b - B_v) + \chi_{nv}\delta(s - S_{nv})\delta(b - B_{nv}). \tag{4}$$

The weights χ_v and χ_{nv} are the probabilities to find the initial system state in the basin of attraction of the vegetated (S_v, B_v) and the nonvegetated fixed points (S_{nv}, B_{nv}), respectively.

III. STOCHASTIC DYNAMIC SYSTEM

We propose a point model for the coupled evolution of soil water saturation, $S[\mathrm{m}^0]$, and plant biomass density, $B[\mathrm{kg\,m}^{-2}]$, based on the deterministic model Eq. (1). The sequence of storm events is modeled as a renewal process that is characterized by a distribution of identical independently distributed interstorm waiting times τ denoted by $\psi_\tau(\tau)$ and a distribution of recharge depth $\xi(s)$ denoted by $p_\xi(\xi;s)$, which depends on the current saturation state. In this sense, the evolution of the system state can be considered a CTRW characterized by nonlinear propagation between turning points, which here are defined by storm events. Storms are modeled as point events, because their duration is typically much shorter than the interstorm waiting time. We first pose the stochastic equations of motion of the saturation and biomass states. In the second part of this section, we derive the set of integro-partial-differential equations that govern the joint PDF of saturation and biomass.

A. A Nonlinear continuous-time random walk of saturation and biomass

Between the nth and $(n+1)$th storm events, the interstorm soil-water saturation S_{is} and biomass B are propagated by the set of coupled stochastic differential equations

$$\frac{dS_{is}}{dt} = -\sigma(S_{is}, B), \tag{5a}$$

$$\frac{dB}{dt} = \beta(S_{is}, B) + \sqrt{2\kappa_b(B)}\,\eta_b(t), \tag{5b}$$

where the initial saturation $S_{is}(t_n)$ is equal to the saturation S_{as} after the storm event, $S_{is}(t_n) = S_{as}(t_n)$; biomass is continuous. The random environmental perturbation in the biomass evolution is modeled as Gaussian white noise η_b. The noise strength is measured by the variance $\kappa_b(B)$, which in general depends on the biomass B, i.e., the Langevin Eq. (5b) is characterized by a multiplicative noise. We use here the Ito interpretation of the stochastic integral [54]. A discussion on the modeling of the noise term as purely additive (κ_b constant), demographic ($\kappa_b \sim B$), or environmental ($\kappa_b \sim B^2$) is given in Ref. [55]. Despite the Gaussianity of η_b, the biomass cannot become negative because we impose the constraint $B > 0$ by a reflecting boundary condition at $B = 0$ for the process Eq. (5b). Notice that the reflecting boundary condition does not preclude the system from evolving toward a system state that is located on the boundary. The saturation S_{as} and clock time t_{n+1} after the $(n+1)$th recharge event are updated according to the recurrence relations

$$S_{as}(t_{n+1}) = S_{is}(t_{n+1}) + \xi_n(S_{is}), \qquad t_{n+1} = t_n + \tau_n, \tag{5c}$$

with the constraint that $S_{is}(t_{n+1}) + \xi_n(S_{is}) \leqslant 1$. Thus, the distribution $p_\xi(\xi;s)$ of the recharge depth takes the form [39]

$$p_\xi(\xi;s) = H(1-s-\xi)\psi_\xi(\xi) + \delta(1-s-\xi)\int_\xi^\infty d\xi''\psi_\xi(\xi''), \tag{6}$$

where $H(x)$ is the Heaviside step function, and $\psi_\xi(\xi)$ is the distribution of precipitation depth. The system of Eqs. (5) represents a CTRW, Eq. (5c), characterized by a nonlinear propagation of the state variables, Eqs. (5a) and (5b), between turning points. Note that Eq. (5a) together with Eq. (5c) can be written in the more compact form

$$\frac{dS}{dt} = -\sigma(S,B) + \sum_{i=1}^{n(t)} \xi_i \delta(t - t_i), \quad n(t) = \max(n | t_n \leqslant t), \tag{7}$$

where the renewal process $n(t)$ counts the number of storm events that occur until time t. For an exponential distribution of interstorm waiting times τ_n [39,44] in Eq. (5c), $n(t)$ is a Poisson process, for a power-law distribution of interstorm waiting times, $n(t)$ denotes a fractional Poisson process [51]. In the

following, we develop the stochastic framework for arbitrary distributions of interstorm waiting times and recharge depth.

The two sources of stochasticity in model Eq. (5) synthesize, within a simple theoretical framework, the multiple sources of variability and randomness present in water-limited ecosystems. Stochastic rainfall, the main forcing in the system, is modeled as a point process. Recharge events due to rainfall are interpreted at the daily time scale, ignoring the temporal structure of individual storms [39,43]; that is, their duration is assumed to be small compared to the lag-time between events. The distributions of interstorm waiting times $\psi_\tau(\tau)$ and precipitation depths $\psi_\xi(\xi)$ incorporate the interannual variability of precipitation patterns. For simplicity, we assume that these distributions model rain through fall, thus incorporating the effect of canopy interception. In addition to random point events due to stochastic rainfall, we have included the effect of small random perturbations in plant biomass. These noise terms model the various sources of variability and randomness in natural ecosystems, from fire to the stochastic nature of vegetation dynamics and fauna populations, as well as damage due to wind, landslides, or runoff water [11].

B. Interstorm waiting time

The behavior of the stochastic dynamic system Eq. (5) depends on the distribution of interstorm waiting times. Recall that this system of equations represents a nonlinear (in the system state) CTRW, whose behaviors can be categorized according to the distribution of waiting times $\psi_\tau(\tau)$.

We first consider a pure power-law distribution of interstorm waiting times such that

$$\psi_\tau(\tau) \sim (\tau/\tau_c)^{-1-a} \tag{8}$$

for $0 < a < 1$, i.e., the mean interstorm waiting time does not exist; τ_c is a characteristic time. Note that such a pure power-law behavior needs to be understood in an asymptotic sense. We do not assume that the power-law behavior persists forever, but describes the storm time series in a certain time regime, or observation window. This type of interstorm waiting time distribution implies that the storm frequency decreases with time. In more detail, the number of storm events up to a certain time t describes the renewal process $n(t) = \min(n|t_n \leqslant t)$ with t_n given by Eq. (5c). The average number $\langle n(t)\rangle$ of storm events up to a time t is then given by the renewal theorem [56] as $\langle n(t)\rangle \sim t^a$. Thus, the frequency f_s of storm events decreases as $f_s(t) = \langle n(t)\rangle/t \sim t^{a-1}$, or, in other words, the typical interstorm waiting time increases with time as t^{1-a}. This implies that the periods without recharge increase, or in other words, the system has ever more time to dry out and evolve toward the nonvegetated state. Specifically, for a finite average recharge depth $\langle\xi\rangle$, the mean precipitation rate is then given by $I(t) = \langle\xi\rangle f_s(t) \sim t^{a-1}$. It decreases with time. Thus, in the long run $I(t) \to 0$ and most systems evolve irrevocably towards a nonvegetated state. Figure 2 shows an ecosystem trajectory for the power-law distribution $\psi(\tau) = a\tau_c^{-1}(1 + x/\tau_c)^{-1-a}$ with $a = 0.6$ and $\tau_c = 10$ and the precipitation depth distribution $\psi_\xi(\xi) = \alpha^{-1}\exp(-\xi/\alpha)$ with $\alpha = 0.016$. The system starts in the vegetated basin and evolves asymptotically toward a succession of nonvegetated states.

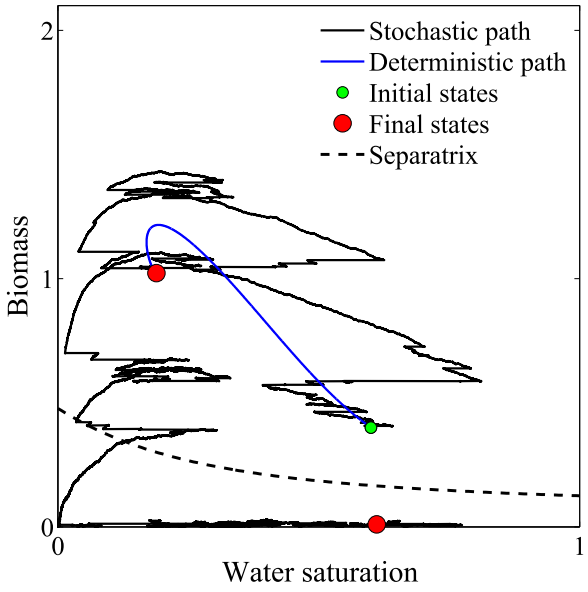

FIG. 2. (Color online) Stochastic ecosystem trajectory for a power-law interstorm waiting time with exponent $a = 0.6$ and characteristic time scale $\tau_c = 10$ and average recharge depth $\alpha = 0.04$ such that $\alpha/\tau_c = 0.004$ is equal to the recharge rate for the deterministic model illustrated in Fig. 1. The remaining model parameters are the same as described in the caption of Fig. 1 with $E = 0.004$. The trajectory starts in the vegetated basin and ends asymptotically in the nonvegetated basin.

For interstorm waiting-time distributions $\psi_\tau(\tau)$, which possess a finite mean $\langle\tau\rangle < \infty$ this is very different. In this case, the average number of storm events increases linearly with time $\langle n(t)\rangle = t/\langle\tau\rangle$. Thus, storms occur with constant frequency $f_s = 1/\langle\tau\rangle$. Accordingly, the mean precipitation rate is constant and given by $I = \langle\xi\rangle/\langle\tau\rangle$. We argue in the next section that the long-time behavior can be fully characterized by the mean interstorm waiting time $\langle\tau\rangle$, or equivalently by the storm frequency $\lambda = 1/\langle\tau\rangle$, and does not depend on the shape of $\psi(\tau)$.

Figure 3 shows two sample trajectories of the stochastic system Eq. (5) that start in the basin of attraction of the vegetated fixed point. Storm events are represented by a Poisson process characterized by the interstorm lag time PDF $\psi_\tau(\tau) = \lambda\exp(-\lambda\tau)$ the precipitation depth distribution is exponential. Figures 3(a) and 3(b) are characterized by the same mean precipitation but different precipitation rates. Figure 3(a) illustrates a system trajectory for a relatively high precipitation rate. The system starts in the nonvegetated basin of the deterministic nonvegetated fixed point. A strong recharge event eventually pushes it over the boarder that separates the vegetated and nonvegetated basins of attraction, where it remains asymptotically. Thus, stochastic fluctuations of the recharge conditions can be beneficial for the ecosystem evolution, or in other words, intermittent strong storm events may push the ecosystem into the basin of the vegetated fixed point. For less frequent recharge events, as illustrated in Fig. 3(b), the opposite is true. Here, the system first evolves toward the vegetated fixed point but then makes a transition into the basin of attraction of the nonvegetated fixed point due

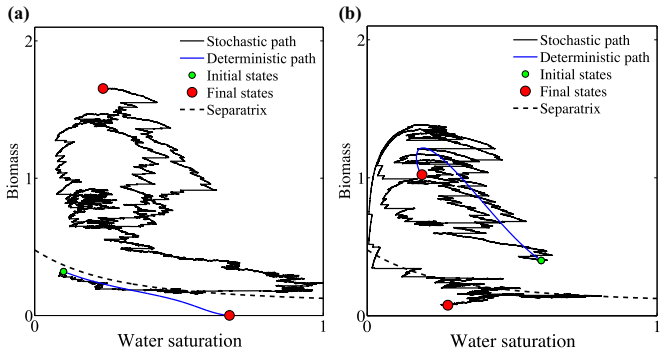

FIG. 3. (Color online) Stochastic ecosystem trajectories for (a) frequent rain events with low amplitude, and (b) rare storm events with large amplitude. The model parameters are the same as in Fig. 1 with $E = 0.004$ and a mean daily preciptation of $I = 0.004$. The mean daily precipitation is the same for both cases, but the mean lag time between storms and mean precipitation depths are different: $\alpha = 0.016$, $\lambda = 1/4$ (a), and $\alpha = 0.04$, $\lambda = 1/10$ (b).

to relatively long interstorm periods. Temporal variability in the environmental forcing can lead to dynamic steady states that do not coincide with either of the deterministic stable configurations.

C. Evolution equations for the joint PDF of saturation and biomass

The dynamic system Eqs. (1) and (5) describe the ecosystem evolution starting from a given initial saturation and vegetation state as illustrated in Figs. 1 and 3. While for the deterministic model, any system evolves toward one of the two stable configurations, for the stochastic system the behavior is more complex: dynamic steady states may exist that do not coincide with either of the two fixed points. This behavior cannot be analyzed by evaluating single-system trajectories because the information on the stochastic structure of the dynamic steady states and the system response to changes in the environmental forcing is encoded in the joint PDF of saturation and biomass. In this section, we derive the governing equations for the joint PDF of saturation and biomass that are equivalent to the stochastic dynamic system Eq. (5). This set of equations forms the basis for the systematic analysis of the ecosystem evolution subject to stochastic forcing.

To derive the evolution equation for the joint PDF, we first consider the evolution of the ecosystem in an interstorm period given by Eqs. (5a) and (5b). Between two storm events at time t_n and time t_{n+1}, the PDF g of possible ecosystems states that start at $[S_{\rm as}(t_n), B_{\rm as}(t_n)] = (s',b')$ is propagated according to the Fokker-Planck equation

$$\frac{\partial g}{\partial t} - \frac{\partial}{\partial s}\sigma g + \frac{\partial}{\partial b}\beta g - \frac{\partial^2}{\partial b^2}\kappa_b g = 0, \tag{9}$$

where $t_n \leqslant t < t_{n+1}$ and $g(s,b,t = t_n|s',b',t_n) = \delta(s - s')\delta(b - b')$. The density g is the Green function of the Fokker-Planck Eq. (9), or in other words, the transition probability from state (s',b') to (s,b) during the time interval $(t - t')$. Notice that g is a function of $(t - t')$ because Eq. (9) is homogeneous in time.

Note that Eq. (9) describes the (deterministic) evolution of the distribution of ecosystems between two stochastic ecosystem states at random times and random initial states. To obtain the PDF $p(s,b,t)$ we average over the stochastic series of precipitation events that drive the ecosystem to the state under consideration, which can be expressed by

$$p(s,b,t) = \left\langle g\left[s,b,t|S_{\rm as}\left(t_{n_t}\right), B_{\rm as}\left(t_{n_t}\right), t_{n_t}\right]\right\rangle. \tag{10}$$

The renewal process $n_t = \max(n|t_n \leqslant t)$ counts the number of steps to arrive at time t following the continuous-time process Eq. (5c). Thus, the right side of Eq. (10) gives the probability to find the system in state (s,b) at time t given that there was a recharge event at any random time t_{n_t} before. Equation (10) can be developed into

$$p(s,b,t) = \int_0^t dt' \int_0^1 ds' \int_0^\infty db' g(s,b,t|s',b',t')R(s',b',t') \times \int_{t-t'}^\infty d\tau \psi_\tau(\tau), \tag{11}$$

where $R(s,b,t)$ is defined by

$$R(b,s,t) = \sum_{n=0}^\infty \langle \delta[s - S_{\rm as}(t_n)]\delta[b - B_{\rm as}(t_n)]\delta(t - t_n)\rangle. \tag{12}$$

It denotes the probability per time that the system has just arrived at system state (s',b') after the last recharge event at time t'. Thus, Eq. (11) can be read as follows. The probability $p(s,b,t)$ to find the system in the saturation biomass state (s,b) at time t is given by the probability per time $R(s',t')$ that the system has just arrived at system state (s',b') after the last recharge event at time t' times the probability $g(s,b,t|s',b',t')$ that the system evolves toward (s,b) times the probability $\Psi(t - t') = \int_{t-t'}^\infty d\tau \psi_\tau(\tau)$ that the time until the next storm event is larger than $t - t'$. Equation (12) can be expanded to

$$R(s,b,t) = p_0(s,b)\delta(t) + \int_0^s ds' p_\xi(s - s'|s')P(s',b,t), \tag{13}$$

where $p_0(s,b)$ is the initial saturation and biomass PDF, and $P(s,b,t)$ is the probability per time that the system is in the state (s,b) right before a recharge event at time t,

$$P(s,b,t) = \sum_{n=0}^\infty \langle g[s,b,t|S_{\rm as}(t_n), B_{\rm as}(t_n), t_n]\delta(t - t_n - \tau_n)\rangle. \tag{14}$$

Thus, Eq. (13) can be read as follows. The probability per time that the system is in state (s,b) right after a recharge event at time t is given by the probability $P(s',b,t)$ that the system is in the state (s',b) right before the recharge event at time t times the probability $p_\xi(s - s'|s')$ of a recharge depth $s - s'$, which brings the system from s' to s. Similar as above, Eq. (14) can be further developed to

$$P(s,b,t) = \int_0^t dt' \int_0^1 ds' \int_0^\infty db' g(s,b,t|s',b',t')R(s',b',t') \times \psi_\tau(t - t'), \tag{15}$$

i.e., the probability per time time $P(s,b,t)$ to arrive at (s,b) right before a storm event at time t is given by the probability $R(s',b',t')$ that the system is in state (s',b') at time t' right after

the last storm event times the probability $g(s,b,t|s',b',t')$ that it makes a transition to state (s,b) at time t times the probability that the inter-storm waiting time is given by $t-t'$.

Derivation of Eq. (11) with respect to time and using Eqs. (13) and (15) gives the following integro-partial-differential equation for $p(s,b,t)$:

$$\frac{\partial p(s,b,t)}{\partial t} - \frac{\partial}{\partial s}\sigma p + \frac{\partial}{\partial b}\beta p - \frac{\partial^2}{\partial b^2}\kappa_b p = R(s,b,t) - P(s,b,t), \tag{16}$$

which is valid for arbitrary distributions $\psi_\tau(\tau)$ of interstorm waiting times and precipitation depth $\psi_\xi(\xi)$. It is similar to the Liouville Eq. (3) except for the last term on the right due to biomass fluctuations, and the source and sink terms on the right side, which account for system changes due to stochastic precipitation. Note that the process Eq. (5) is in general non-Markovian if the interstorm waiting time τ_n in Eq. (5c) is not Poissonian. In the following, we will analyze the joint saturation and biomass dynamics for the simplified system of Poissonian interstorm waiting times and an exponential distribution of recharge depth.

1. *Poissonian interstorm waiting time*

As discussed in Sec. III B, for waiting time distributions with an infinite mean, the mean precipitation rate I is not constant, but decreases with time, which leads to an evolution of the ecosystem states toward the nonvegetated basin. In the following, we want to discuss the ecosystem behavior under amplification of the hydrologic cycle, which means variability of the storm frequency and depth under a constant mean precipitation rate. Therefore, we focus on $\psi_\tau(\tau)$, which are characterized by a finite mean waiting time, and specifically on an exponential distribution.

As indicated in Sec. III B, we argue that the long-time system behavior can be characterized in terms of the mean interstorm waiting time $\langle\tau\rangle$. To show this, we consider a sharply peaked $\psi(\tau)$ characterized by finite mean $\langle\tau\rangle$ and variance $\sigma_\tau^2 = \langle(\tau - \langle\tau\rangle)^2\rangle$. Thus, we may approximate

$$\int_0^\infty d\tau\, H(\tau - t)\psi_\tau(\tau) = H(\langle\tau\rangle - t) + \cdots, \tag{17}$$

where the dots denote subleading contributions for $t \gg \langle\tau\rangle$. This relation is exact for $\psi(\tau) = \delta(t - \langle\tau\rangle)$. Using this approximation in Eq. (11) gives for $t \gg \langle\tau\rangle$

$$p(s,b,t) \approx \langle\tau\rangle \int_0^1 ds' \int_0^\infty db' g(s,b,t|s',b',t - \langle\tau\rangle) \times R(s',b',t - \langle\tau\rangle). \tag{18}$$

Similarly, we obtain for Eq. (15)

$$P(s,b,t) = \int_0^1 ds' \int_0^\infty db' g(s,b,t|s',b',t - \langle\tau\rangle) \times R(s',b',t - \langle\tau\rangle). \tag{19}$$

Comparing Eqs. (18) and (19), we obtain the relation

$$P(s,b,t) = \lambda p(s,b,t), \tag{20}$$

with $\lambda = \langle\tau\rangle^{-1}$ the constant storm frequency. This relation is exact if the stochastic rainfall is a Poisson process, i.e., for exponentially distributed interstorm waiting times [43],

$$\psi_\tau(\tau) = \lambda \exp(-\lambda\tau), \tag{21}$$

with λ the constant frequency of storm events. Inserting the latter into Eqs. (11) and (13), we immediately obtain the identity Eq. (20). Using Eq. (20) in Eq. (13), we obtain directly

$$R(s,b,t) = \delta(s - S_0)\delta(b - B_0)\delta(t) + \lambda \int_0^s ds' p_\xi(s - s'|s')p(s',b,t). \tag{22}$$

Inserting Eqs. (20) and (22) into Eq. (16) gives the following Master equation for $p(s,b,t)$:

$$\frac{\partial p(s,b,t)}{\partial t} - \frac{\partial}{\partial s}\sigma p + \frac{\partial}{\partial b}\beta p - \frac{\partial^2}{\partial b^2}\kappa_b p = \lambda \int_0^s ds' p_\xi(s - s'|s')p(s',b,t) - \lambda p. \tag{23}$$

Using now the explicit Eq. (6) for the conditional recharge depth, we obtain

$$\frac{\partial p(s,b,t)}{\partial t} - \frac{\partial}{\partial s}\sigma p + \frac{\partial}{\partial b}\beta p - \frac{\partial^2}{\partial b^2}\kappa_b p = \lambda \int_0^s ds' \psi_\xi(s - s')p(s',b,t) - \lambda p, \tag{24}$$

for $0 < s < 1$ and $0 < b < \infty$. The boundary conditions are given by

$$p(0,b,t) = 0,$$
$$p(1,b,t) = \frac{\lambda}{\sigma(1,b)} \int_0^1 ds' \int_{1-s'}^\infty d\xi\, \psi_\xi(\xi)p(s',b,t), \tag{25}$$

and zero probability flux at the boundaries at $b = 0$ and ∞.

2. *Exponentially distributed recharge depth*

Furthermore, we assume that the nondimensional recharge depth is exponentially distributed [39]:

$$\psi_\xi(\xi) = \exp(-\xi/\alpha)/\alpha. \tag{26}$$

Thus, the mean precipitation rate then is given by $I = \alpha\lambda$. With these choices, Eq. (24) becomes

$$\frac{\partial p}{\partial t} - \frac{\partial}{\partial s}\sigma p + \frac{\partial}{\partial b}\beta p - \frac{\partial^2}{\partial b^2}\kappa_b p = \frac{\lambda}{\alpha} \int_0^s ds' \exp\left(-\frac{s - s'}{\alpha}\right) p(s',b,t) - \lambda p. \tag{27}$$

Furthermore, for $\alpha \ll 1$, the boundary condition Eq. (25) at $s = 1$ can be simplified to the Robin boundary condition:

$$[\sigma(1,b) - \alpha\lambda]p(1,b,t) + \alpha^2\lambda \frac{\partial p(1,b,t)}{\partial s} = 0. \tag{28}$$

The joint PDF of saturation and biomass at steady state, $p_\infty(s,b) = \lim_{t\to\infty} p(b,s,t)$, provides a map of possible ecosystem states and their control by the stochastic driving forces.

We solve these equations numerically, using high-order finite differences for the spatial derivatives, Simpson's rule to approximate the integral, and a third-order Runge-Kutta scheme for the time integration.

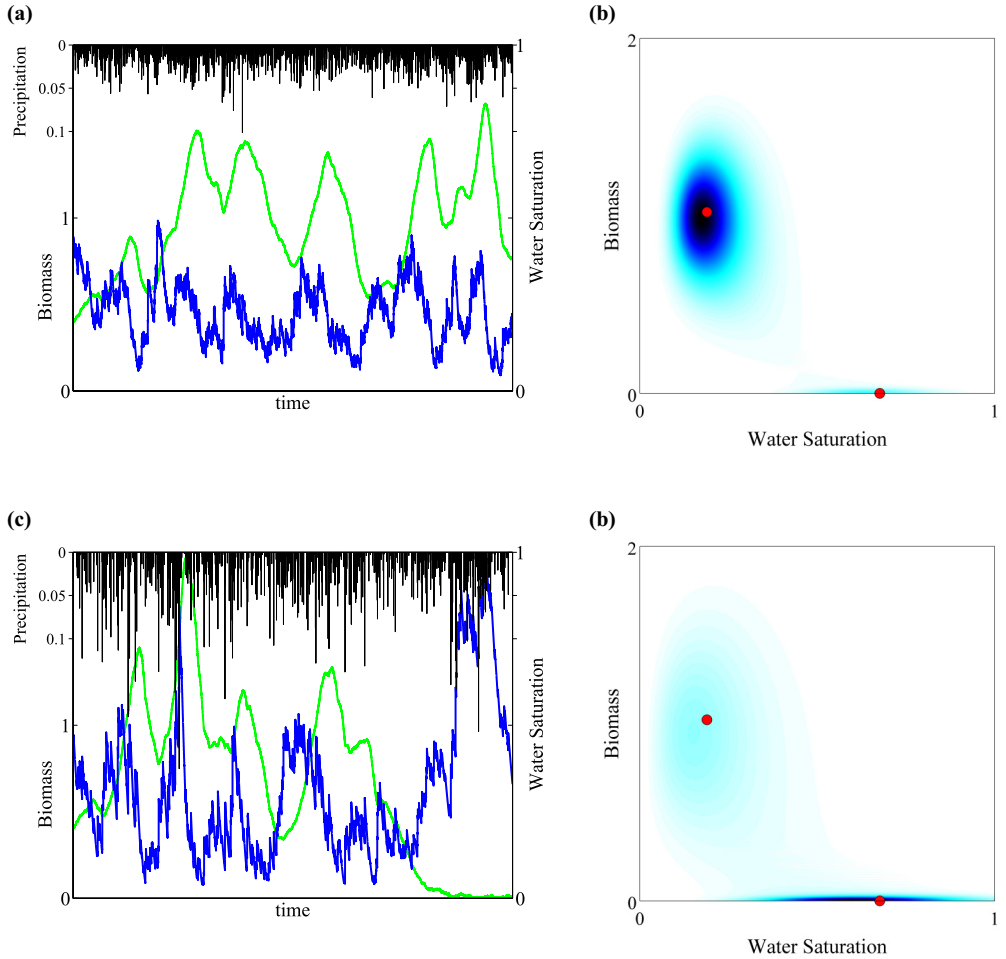

FIG. 4. (Color online) (a), (c) Sample realizations of the model Eqs. (5a) and (5b), coupling rainfall, soil moisture, and vegetation biomass with stochastic rainfall and Gaussian perturbations. The model parameters are the same as described in the caption of Fig. 1, with $E = 0.004$ and the mean daily precipitation $I = 0.004$. In these two scenarios, the mean annual precipitation is the same, but the mean lag time between storms and mean precipitation depths are different: $\alpha = 0.012$, $\lambda = 1/3$ (cases a and b), and $\alpha = 0.032$, $\lambda = 1/8$ (cases c and d). (b), (d) Steady-state joint probability density functions of soil moisture and biomass, calculated with our stochastic model, Eq. (27). In the case of frequent, small storm events, the PDF has a clear maximum around the vegetated stable state (b). In contrast, for infrequent, larger precipitation events, the probability of the nonvegetated system states increases (d). The cumulative probability to be in the vegetated basin is 0.92 for scenario 1 (b) and 0.6 in scenario 2 (d).

IV. STOCHASTIC ANALYSIS OF THE WATER-VEGETATION SYSTEM

The key questions we address in this section are: how the stochastic forcing impacts the distribution of possible ecosystem states; and how changes in the temporal variability of the stochastic drivers of the ecosystem due to intensification of the hydrologic cycle induce transitions between system states. To this end, we first establish an evolution equation for the joint PDF of saturation and biomass, then discuss the noise-induced system organization, before we analyze the resilience of the stochastic system due to external fluctuations.

A. Bistability and bimodality

The dynamics of the deterministic system Eq. (1) drive the ecosystem toward either of the two stable states. The PDF evolves from a given distribution of initial system states $p(s,b,t = 0) = p_0(s,b)$ toward the steady PDF Eq. (4). The system is *bistable* and exhibits memory of the distribution of initial system states through the weights χ_v and χ_{nw}. This *bistability* in the underlying deterministic dynamics translates into *bimodality* for the PDF of the stochastic system Eq. (5). The stochastic system reaches asymptotically a steady state, which is independent of the distribution of initial system states; it has no memory. The system self-organizes into a dynamic steady state that is fully determined by the stochastic forcings.

Figure 4 illustrates the bimodal system PDF for two different stochastic forcings, which are characterized by the same mean precipitation rate $I = \alpha_i \lambda_i$, where $i = 1, 2$ for systems 1 and 2. Figure 5 shows the same PDFs obtained from Monte Carlo simulations. System 1 has a higher precipitation frequency λ_1 and lower mean amplitude α_1 than system 2. The difference between the two different stochastic forcings is illustrated in Figs. 4(a) and 4(c), which show individual realizations of the respective stochastic precipitation series, and the resulting evolutions of saturation and biomass. The fluctuations in saturation and biomass are significantly smaller in system 1 than in system 2. System 2 eventually evolves

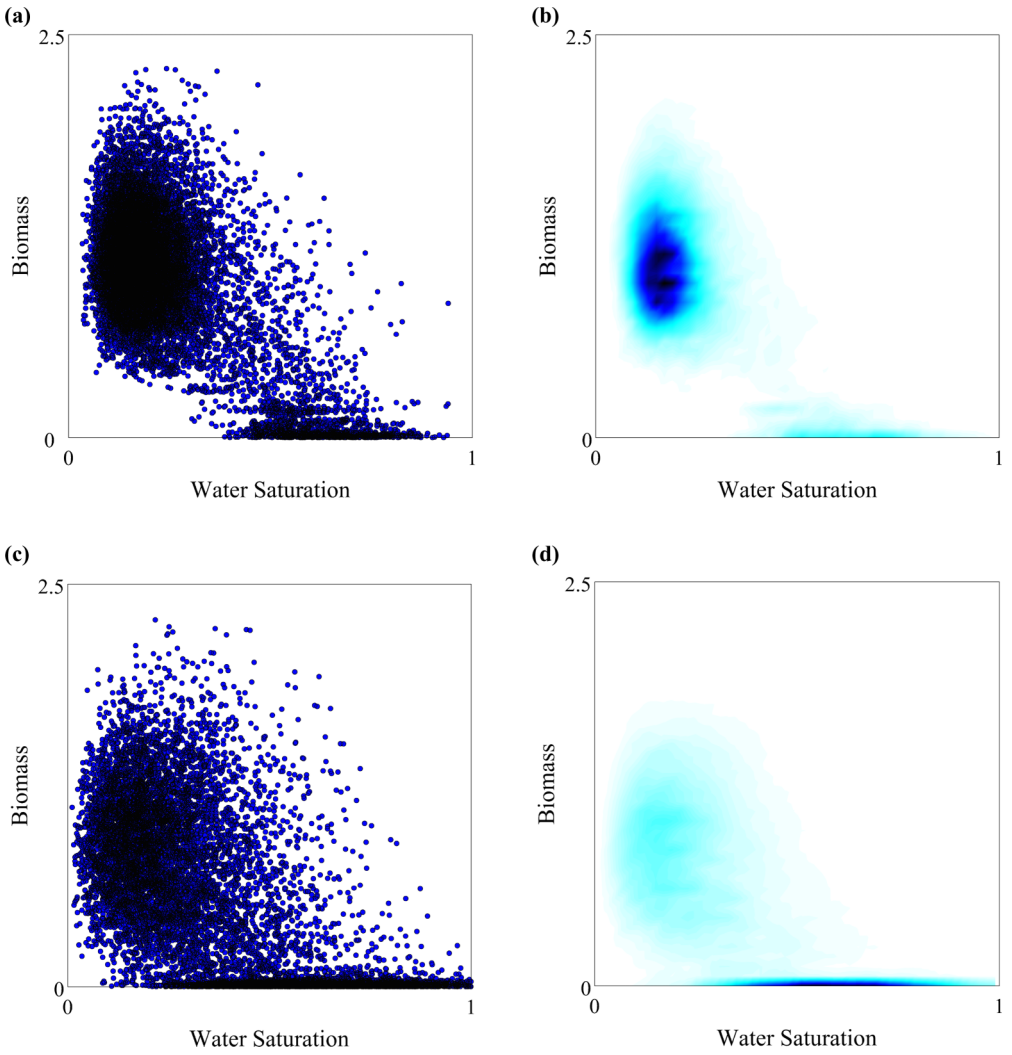

FIG. 5. (Color online) Empirical joint probability density functions from Monte Carlo simulation of the model Eqs. (5a) and (5b) for the same scenarios as described in the caption of Fig. 4. (b), (d) Steady-state joint probability density functions of soil moisture and biomass as in Fig. 4. (a), (c) Scatter plot of system states during the time evolution of soil moisture and biomass. Right panels, normalized histograms of system states.

to a nonvegetated state, unlike system 1, which fluctuates around a vegetated state. The PDF Eq. (4) of the corresponding determinisitic model is identical for the two models, and, as outlined above, depends solely on the distribution of initial system states. The PDFs of the stochastic systems 1 and 2 do not depend on the initial system distribution. They depend solely on the stochastic forcing, the *intensity* of the hydrologic cycle as expressed by the precipitation frequency and average precipitation depth. System 1 develops a bimodal PDF whose weight is concentrated about the vegetated state. The cumulative probability for a system to be in the vegetated basin here is 0.92. In this scenario, intermittent precipitation turns out to be better for the ecosystem to evolve toward a vegetated state. The mechanism is illustrated in the single ecosystem trajectory shown in Fig. 3(a). A strong recharge event may push the ecosystem over the separatrix between the nonvegetated and the vegetated basins. This is changed in scenario 2, which is characterized by less frequent precipitation events with higher precipitation depth. Here an ecosystem has a higher probability to develop toward a nonvegetated state. In fact, the probability to be in the vegetated basin here is reduced to 0.6. Note that the main driver here is the frequency of storm events or mean interstorm waiting time. As the interstorm waiting time increases, the system has more time to "dry out," i.e., to evolve toward the nonvegetated basin. This cannot be compensated for by the increased precipitation depth due to the finite carrying capacity of the soil. These dynamics are illustrated for a single ecosystem trajectory in Fig. 3(b).

It is interesting to further consider the system fluctuations observed in Fig. 4 for the different stochastic driving forces. Figures 6(a) and 6(b) show biomass time series for systems 1 and 2. As the hydrologic cycle intensifies, which means less frequent storm events with a higher amplitude, the trajectory of the ecosystem shows intermittent behavior. Large fluctuations in saturation and biomass precede system transitions from mostly vegetated to nonvegetated states. Reference [57] observed that the occurrence of increased system fluctuations may serve as an indicator for critical ecosystem transitions. Here it turns out that the evolution is in fact intermittent. Large system fluctuations are followed by quiet periods

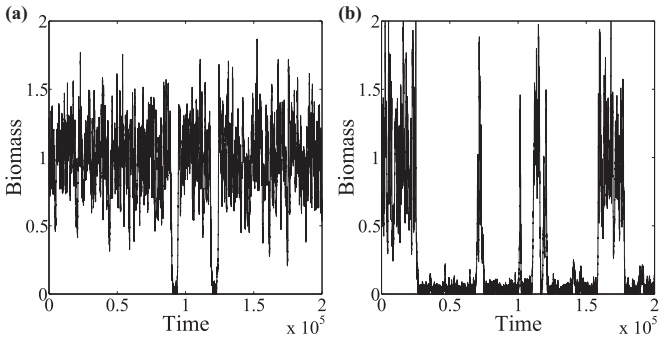

FIG. 6. Long-time biomass time series for the systems described in the caption of Fig. 4. The shift from the vegetated to the nonvegetated state leads to larger system fluctuations and intermittent behavior. The model parameters are the same as in Fig. 4. In these two scenarios, the mean annual precipitation is the same, but the mean lag time between storms and mean precipitation depths are different: $\alpha = 0.012$, $\lambda = 1/3$ (case a), and $\alpha = 0.032$, $\lambda = 1/8$ (case b).

around the nonvegetated state before the system recovers and starts fluctuating again. The shift from the vegetated to the nonvegetated ecosystem is concurrent with an increase of the length of interstorm periods, which drive the system toward the nonvegetated state, and an increase in recharge depth, which has the opposite affect. This interaction leads to the increased system fluctuations and the intermittent behavior observed in Fig. 6.

B. Stochastic resilience

As discussed above, the structural properties of the joint PDF of saturation and biomass vary drastically with the stochastic structure of rainfall forcing, even if the mean annual precipitation does not change, as shown in Fig. 4. For relatively frequent small precipitation events, the system will be most likely observed in the vicinity of the vegetated attractor; see Figs. 4(a) and 4(b). With increasing mean interstorm periods and precipitation depth, one observes a transition towards a preferentially nonvegetated state; see Figs. 4(c) and 4(d).

We characterize the resilience of the water-vegetation system through an effective potential function [29,36]. Potential analysis has been successfully used in climate modeling and ecology, from detecting climate states from time series analysis [29] and identifying multiple stable states of woody cover [25], to elucidating the impact of soil-atmosphere feedbacks on the dynamics of soil moisture [36]. Resilience describes how stable the stochastic dynamic system (defined by its intrinsic fluctuations in terms of storm frequency and depth, and biomass) is in response to an external perturbation. To this end, we define the effective potential [54] $U(s,b) = -\ln p_\infty(s,b)$ in terms of the steady-state PDF of saturation and biomass. The gradient of this potential can be seen as a phenomenological force that describes the way the stochastic system responds to an external fluctuation. Notice that the effective potential quantifies the effective dynamics of the system. It does not reproduce the exact system transients but defines an effective stochastic dynamic system that evolves toward the same steady state. Figure 7 shows the effective potential functions for systems 1 and 2 along with sample trajectories determined from Eq. (5). The sample trajectories are consistent with the topography of the potential functions.

The effective potentials are bimodal, reflecting the steady-state PDF. The depth of the vegetated potential well is a measure for the resilience of the system-to-system changes toward the nonvegetated state. The topography of the effective potential is related to a critical slowing down due to flattening of the potential around the wells, which strengthens or weakens depending on the rainfall forcing and ecosystem parameters. For frequent precipitation events of small amplitude, the steady-state PDF has an essentially unimodal structure [Fig. 4(b)]. Accordingly, the effective potential corresponding to frequent, small rainfall events [Fig. 7(a)] exhibits a steep well around the vegetated state, which indicates a fast recovery from extrinsic perturbations when in the vegetated state. There is only a flat well around the nonvegetated state. For infrequent events of larger amplitude [Fig. 4(d)], the PDF shifts toward a dominant unimodal distribution around the nonvegetated state. The corresponding effective potential for infrequent, large events [Fig. 7(b)] has a broad and shallow well around the

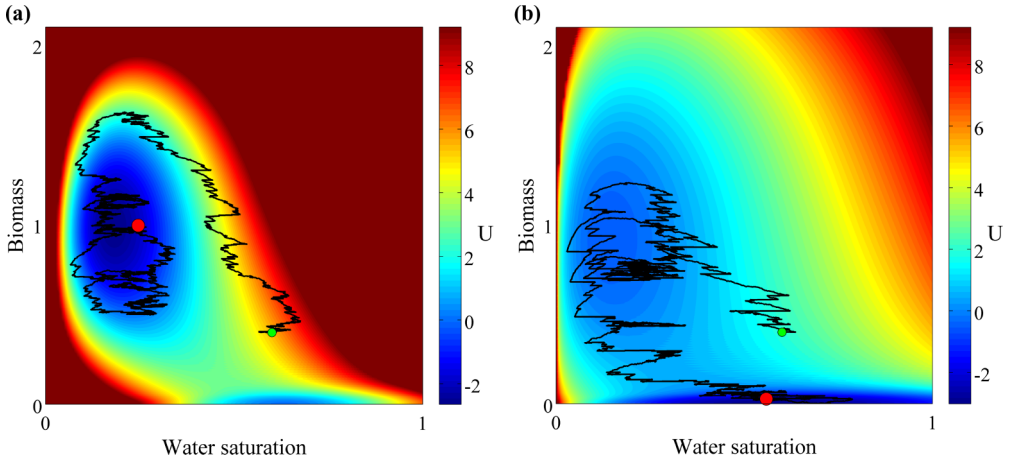

FIG. 7. (Color online) Quantifying resilience using effective potential analysis. The effective potentials reflect the effective system dynamics for mean daily precipitation $\alpha \times \lambda = 0.004$ and (left) frequency of storms $\lambda = 1/2$ and (right) $\lambda = 1/10$. Superposed are sample trajectories determined from Eq. (5) for the same model parameters as described in the caption of Fig. 4.

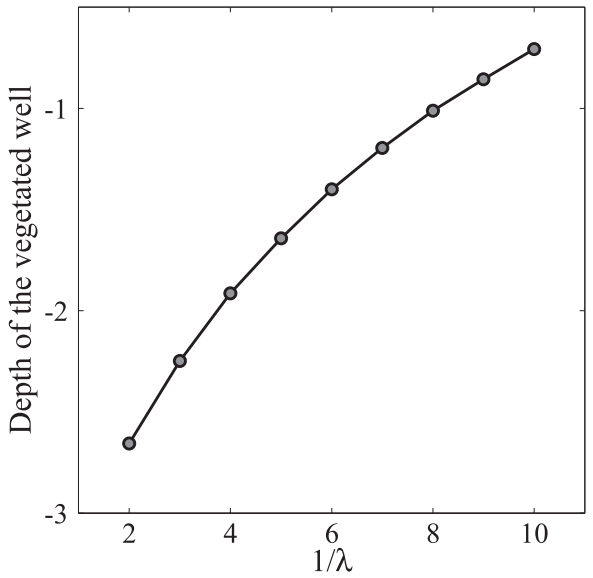

FIG. 8. Depths of the vegetated well for $\alpha \times \lambda = 0.004$ as a function of the mean interstorm waiting time $1/\lambda$. The model parameters are the same as described in the caption of Fig. 4. The depth of the well can be interpreted as the attracting strength of the vegetated state and is a measure of its resilience against random perturbations. In the case of shallow wells, which are characteristic of the larger events separated by larger intervening periods [large λ, Fig. 7(b)] the system can easily fall into the basin of attraction of the nonvegetated state. These systems are also characterized by higher variability and intermittency [Fig. 6(b)].

vegetated state, and a deep, steep well around the nonvegetated state, which, however, covers a relatively small area in phase space. This structure suggests on one hand a slow recovery from perturbations in the vegetated areas, and on the other hand the possibility of large fluctuations when perturbed from the nonvegetated state due to the small area covered by the nonvegetated mode. This is also reflected in the intermittent behavior of the biomass trajectories illustrated in Fig. 6.

Figure 8 shows the well strength measured by its depth, depending on the mean interstorm waiting time $1/\lambda$. The strength of the vegetated well decreases as the hydrologic cycle intensifies, i.e., as $1/\lambda$ increases. We conclude that an increased variability in rainfall patterns, even with constant mean annual precipitation, leads to a higher probability of observing the system in a nonvegetated state and to a loss in resilience of vegetated states.

V. CONCLUSIONS

Through stochastic modeling of the coupled dynamics of soil moisture and vegetation dynamics, we find that the structure of rainfall, not just the mean precipitation rate, is the key determinant of the state of the system. Our results suggest transitions in the steady-state joint PDF of soil moisture and vegetation biomass when the structure of rainfall changes, even if the mean precipitation rate does not change. The relationship between bistability and bimodality of the joint PDF depends on the underlying water-biomass coupling and on the rainfall statistics. We quantify the impact of rainfall variability on ecosystem resilience and find that resilience of vegetated ecosystem states decreases with increasing intensification of the hydrologic cycle. Our results point to the need to contextualize global datasets of climate, soil moisture, and vegetation in terms of both aggregate precipitation measures and the patterns of inter- and intraannual rainfall variability.

ACKNOWLEDGMENTS

M.D. acknowledges the support of the European Research Council through the project MHetScale (Grant No. 617511). L.C.F. gratefully acknowledges a "Ramón y Cajal" Fellowship from the Spanish Ministry of Economy and Competitiveness (Grant No. RyC-2012-11704).

[1] D. R. Easterling, G. A. Meehl, C. Parmesan, S. A. Changnon, T. R. Karl, and L. O. Mearns, Science **289**, 2068 (2000).
[2] A. K. Knapp *et al.*, Bioscience **58**, 811 (2008).
[3] I. M. Held and B. J. Soden, J. Clim. **19**, 5686 (2006).
[4] P. Y. Groisman, R. W. Knight, D. R. Easterling, T. R. Karl, G. C. Hegerl, and V. N. Razuvaev, J. Clim. **18**, 1326 (2005).
[5] R. P. Allan and B. J. Soden, Science **321**, 1481 (2008).
[6] B. N. Goswami, V. Venugopal, D. Sengupta, M. S. Madhusoodanan, and P. K. Xavier, Science **314**, 1442 (2006).
[7] P. Y. Groisman and R. W. Knight, J. Clim. **21**, 1850 (2008).
[8] J. L. Heisler-White, J. M. Blair, E. F. Kelly, K. Harmoney, and A. K. Knapp, Global Change Biol. **15**, 2894 (2009).
[9] S. P. Good and K. K. Caylor, Proc. Natl. Acad. Sci. USA **108**, 4902 (2011).
[10] M. Holmgren, M. Hirota, E. H. V. Nes, and M. Scheffer, Nature Clim. Change **3**, 755 (2013).
[11] C. S. Holling, Annu. Rev. Ecol. Syst. **4**, 1 (1973).
[12] C. Folke, S. Carpenter, B. Walker, M. Scheffer, E. T, L. Gunderson, and C. Holling, Annu. Rev. Ecol. Evol. Syst. **35**, 557 (2004).
[13] T. M. Lenton, H. Held, E. Kriegler, J. W. Hall, W. Lucht, S. Rahmstorf, and H. J. Schellnhuber, Proc. Natl. Acad. Sci. USA **105**, 1786 (2008).
[14] I. Noy-Meir, J. Ecol. **63**, 459 (1975).
[15] R. M. May, Nature **269**, 471 (1977).
[16] W. H. Schlesinger, J. F. Reynolds, G. L. Cunningham, L. F. Huenneke, W. M. Jarrell, R. A. Virginia, and W. G. Whitford, Science **247**, 1043 (1990).
[17] M. Scheffer, J. Bascompte, W. A. Brock, V. Brovkin, S. R. Carpenter, V. Dakos, H. Held, E. H. van Nes, M. Rietkerk, and G. Sugihara, Nature **461**, 53 (2009).
[18] M. Scheffer *et al.*, Science **338**, 344 (2012).

[19] B. H. Walker, D. Ludwig, C. S. Holling, and R. M. Peterman, J. Ecol. **69**, 473 (1981).
[20] P. S. Eagleson and R. I. Segarra, Water Resour. Res. **21**, 1483 (1985).
[21] T. M. Lenton, Nature Climate Change **1**, 201 (2011).
[22] I. Noy-Meir, Annu. Rev. Ecol. Syst. **4**, 25 (1973).
[23] M. Rietkerk, M. C. Boerlijst, F. van Langevelde, R. HilleRisLambers, J. van de Koppel, L. Kumar, H. H. T. Prins, and A. M. de Roos, Am. Nat. **160**, 524 (2002).
[24] M. Rietkerk, S. C. Dekker, P. C. de Ruiter, and J. V. de Koppel, Science **305**, 1926 (2004).
[25] M. Hirota, M. Holmgren, E. H. Van Nes, and M. Scheffer, Science **334**, 232 (2011).
[26] A. C. Staver, S. Archibald, and S. A. Levin, Science **334**, 230 (2011).
[27] A. R. Ives, Ecol. Monogr. **65**, 217 (1995).
[28] V. Guttal and C. Vayaprakash, Ecol. Model. **201**, 420 (2007).
[29] V. N. Livina, F. Kwasniok, and T. M. Lenton, Clim. Past **6**, 77 (2010).
[30] S. Bathiany, M. Claussen, and K. Fraedrich, Clim. Dynam. **38**, 1775 (2012).
[31] P. D'Odorico, F. Laio, and L. Ridolfi, Proc. Natl. Acad. Sci. USA **102**, 10819 (2005).
[32] R. Vezzoli, C. De Michele, H. Pavlopoulos, and R. J. Scholes, Phys. Rev. E **77**, 051908 (2008).
[33] M. Parker, A. Kamenev, and B. Meerson, Phys. Rev. Lett. **107**, 180603 (2011).
[34] M. Baudena and A. Provenzale, Hydrol. Earth Syst. Sci. **12**, 679 (2008).
[35] I. Rodriguez-Iturbe, D. Entekhabi, and R. L. Bras, Water Resour. Res. **27**, 1899 (1991).
[36] D. Entekhabi, I. Rodriguez-Iturbe, and R. L. Bras, J. Climate **5**, 798 (1992).
[37] P. D'Odorico and A. Porporato, Proc. Natl. Acad. Sci. USA **101**, 8848 (2004).
[38] J. Yin, A. Porporato, and J. Albertson, Water Resour. Res. **50**, 6053 (2014).
[39] I. Rodriguez-Iturbe, A. Porporato, L. Ridolfi, V. Isham, and D. R. Cox, Proc. R. Soc. Lond. A **455**, 3789 (1999).
[40] G. Katul, A. Porporato, and R. Oren, Annu. Rev. Ecol. Evol. Syst. **38**, 767 (2007).
[41] I. Rodriguez-Iturbe, P. D'Odorico, A. Porporato, and L. Ridolfi, Water Resour. Res. **35**, 3709 (1999).
[42] F. Laio, A. Porporato, L. Ridolfi, and I. Rodriguez-Iturbe, Adv. Water Res. **24**, 707 (2001).
[43] I. Rodriguez-Iturbe and A. Porporato, *Ecohydrology of Water-Controlled Ecosystems: Soil Moisture and Plant Dynamics* (Cambridge University Press, Cambridge, 2004).
[44] E. Daly and A. Porporato, Phys. Rev. E **81**, 061133 (2010).
[45] E. Zea-Cabrera, Y. Iwasa, S. Levin, and I. Rodriguez-Iturbe, Water Res. Res. **42**, W06D02 (2006).
[46] J. M. Nordbotten, I. Rodriguez-Iturbe, and M. A. Celia, Water Res. Res. **43**, W01408 (2007).
[47] E. W. Montroll and G. H. Weiss, J. Math. Phys. **6**, 167 (1965).
[48] H. Scher and M. Lax, Phys. Rev. B **7**, 4491 (1973).
[49] R. Metzler and J. Klafter, Phys. Rep. **339**, 1 (2000).
[50] B. Berkowitz, A. Cortis, M. Dentz, and H. Scher, Rev. Geophys. **44**, RG2003 (2006).
[51] N. Laskin, Commun. Nonlinear Sci. Numer. Simul. **8**, 201 (2003).
[52] P. S. Eagleson, Water Resour. Res. **14**, 705 (1978).
[53] E. A. Coddington and N. Levinson, *Theory of Ordinary Differential Equations* (McGraw-Hill, New York, 1955).
[54] H. Risken, *The Fokker-Planck Equation: Methods of Solution and Applications* (Springer-Verlag, Berlin/Heidelberg, 1996).
[55] M. Kaluzhny, E. Seri, R. Chocron, C. H. Flather, R. Kadmon, and N. M. Shnerb, Am. Nat. **184**, 439 (2014).
[56] W. Feller, *An Introduction to Probability Theory and Its Applications*, Vol. II (John Wiley & Sons, New York, 1970).
[57] S. R. Carpenter and W. A. Brock, Ecol. Lett. **9**, 311 (2006).